Synthesis, Structure, and Electronic Properties of $LaCa_2Mn_2O_7$

M. A. Green*

Davy Faraday Research Laboratory, Royal Institution of Great Britain, 21 Albemarle Street, London, W1X 4BS United Kingdom

D. A. Neumann

NIST Centre for Neutron Research, National Institute of Standards and Technology, Gaithersburg, Maryland 20899

Received July 5, 1999. Revised Manuscript Received October 14, 1999

Synthesis of the Ruddlesden−Popper phase, $LaCa_2Mn_2O_7$ is presented. The difficulty in obtaining a single-phase material, free from a perovskite impurity, is highlighted. Powder X-ray diffraction indicates an orthorhombic symmetry. Powder neutron diffraction reveals a subtle rotation of the MnO_6 octahedra and reduction of symmetry to a C-centered orthorhombic cell (*Cmcm*). Cation ordering occurs with the larger La ions adopting the 12-coordinated site within the perovskite block and the smaller Ca ions situated in the 9-coordinated site in the rock salt layer. Magnetization measurements indicate a weak ferromagnetic transition at around 250 K, which is assigned to a perovskite impurity of 11.4%, as determined by neutron diffraction. Low-temperature neutron diffraction measurements confirms ferromagnetic ordering in the perovskite impurity and show no indication of long-range magnetic ordering in the majority Ruddlesden−Popper phase. Magnetotransport measurements show a metal−insulator transition at around 150 K and magnetoresistance up to 320 K. However, the perovskite impurity limits confidence in the assignment of the origin of the magnetoresistance effect.

Introduction

Colossal magnetoresistance (CMR) in mixed-valent Mn^{3+}/Mn^{4+} oxides has attracted considerable interest due to its potential application in magnetic storage and sensing devices. Much of this work has focused on the perovskite systems with the general formula, $AMnO_3$ (A = alkali earth metal or lanthanide),[1,2] where the composition of A greatly influences the electronic properties. Many compositions are characterized by a ferromagnetic transition which is explained by Zener's double-exchange theory.[3] In this mechanism, the increase in kinetic energy gained by the delocalization of e_g^1 electrons overcomes the antiferromagnetic coupling between localized t_{2g}^3 electrons ($S = {}^3/_2$), creating a ferromagnetic state. Application of a magnetic field at a temperature just above T_c results in field-induced ordering of the t_{2g}^3 electrons, thereby reducing the spin-disorder scattering of the e_g^1 electrons and producing negative magnetoresistance. The functionality of these materials as industrial devices is often hindered by the high magnetic fields and/or the low temperatures required for significant magnetoresistance effects to be observed. More recently, work has extended into other structure types to gain a greater insight into the various competing electronic interactions as well as to overcome these technological problems. In particular, one of these structure types, the layered Ruddlesden−Popper phases with general formula, $A_{n+1}Mn_nO_{3n+1}$, has opened up new opportunities for tailoring the Mn−O interaction and tuning the resultant properties.[4−7] The n MnO_2 sheets are separated by a rock-salt type layer giving quasi-two-dimensional properties. $La_{1+x}Sr_{2-x}Mn_2O_7$ has a metal−insulator transition at its ferromagnetic ordering temperature and show a significant magnetoresistance effect, which is reminiscent of the perovskite systems.[4,5,8,9] Substitution of a smaller lanthanide ion for La in $La_{1+x}Sr_{2-x}Mn_2O_7$ dramatically reduces the influence of the double exchange. However, despite $Nd_{1+x}Sr_{2-x}Mn_2O_7$ being antiferromagnetic and showing neither ferromagnetism nor a metal−insulator transition, it still displays colossal magnetoresistance.[10,11] Greatly reducing the average lanthanide cation size destroys all long-range magnetic order,[12,13] as in $HoSr_2Mn_2O_7$, which

(1) Rao, C. N. R.; Mahesh, R. *Curr. Opin. Solid State Mater. Sci.* **1997**, *2*, 32.
(2) Rao, C. N. R.; Cheetham, A. K.; Mahesh, R. *Chem. Mater.* **1996**, *8*, 2421.
(3) Zener, C. *Phys. Rev.* **1951**, *82*, 1963.
(4) Moritomo, Y.; Asamitsu, A.; Kuwahara, H.; Tokura, Y. *Nature* **1996**, *380*, 141.
(5) Battle, P. D.; Green, M. A.; Laskey, N. S.; Millburn, J. E.; Rosseinsky, M. J.; Sullivan, S. P.; Vente, J. F. *Chem. Commun.* **1996**, 767.
(6) Mahesh, R.; Mahendiran, R.; Raychaudhuri, A. K.; Rao, C. N. R. *J. Solid State Chem.* **1996**, *122*, 448.
(7) Kimura, T.; Tomioka, Y.; Kuwahara, H.; Asamitsu, A.; Tamura, M.; Tokura, Y. *Science* **1996**, *274*, 1698.
(8) Battle, P. D.; Cox, D. E.; Green, M. A.; Millburn, J. E.; Spring, L. E.; Radaelli, P. G.; Rosseinsky, M. J.; Vente, J. F. *Chem. Mater.* **1997**, *9*, 1042.
(9) Mitchell, J. F.; Argyriou, D. N.; Jorgensen, J. D.; Hinks, D. G.; Potter, C. D.; Bader, S. D. *Phys. Rev. B−Condens. Matter* **1997**, *55*, 63.

10.1021/cm991094i CCC: $19.00
Published on Web 12/23/1999

also shows a structural phase transition to a primitive $P4_2/mnm$ cell.[14] Studies of the analogous $La_{1+x}Ca_{2-x}Mn_2O_7$ series have reported $I4/mmm$ tetragonal symmetry and a ferromagnetic transition at around 250 K, but it is distinguished from other systems by having a large magnetoresistance effect only at temperatures much below the magnetic-ordering temperature.[15−19]

In this present study, the synthesis, structure, and electronic properties of the $x = 0$ member of the $La_{1+x}Ca_{2-x}Mn_2O_7$ series were investigated by a combination of techniques. It is found that the initial product formed during synthesis has the perovskite structure and only after extended heating does a layered structure form. The coincidental similarity between the X-ray diffraction patterns of the Ruddlesden−Popper and perovskite phase make phase purity difficult to ascertain. Neutron diffraction data clearly indicates that despite rigorous precautions taken during synthesis, a small perovskite impurity remains. It is this impurity which is assigned to be the cause of the weak ferromagnetic transition at 250 K, which is confirmed by low-temperature neutron diffraction. Magnetic scattering was not observed in the Ruddlesden−Popper phase, implying an absence of long-range magnetic order.

Experimental Section

Stoichiometric amounts of La_2O_3, $CaCO_3$, and MnO_2 were mixed and fired at 1100 °C for 24 h. Samples were ground, pelletized, and heated at 1350 °C in air with intermediate regrinding every 24 h. X-ray diffraction was performed using a Siemens D500 fitted with a primary monochromator giving Cu $K\alpha_1$ radiation at $\lambda = 1.54056$ Å. High-resolution X-ray diffraction data was taken with slits sizes of 1°, 1° (presample) and 0.1°, 0.015° (postsample) from 5° to 90° with a 0.02° step size and count time of 25 s per step. Neutron diffraction measurements were performed on a 10-g sample in a vanadium container on the BT1 diffractometer at the National Institute of Standards and Technology (NIST), Gaithersburg, MD, using a Cu (311) monochromator ($\lambda = 1.5401$ Å) and 14′ final collimator. Scans were taken from 3° to 165° with a step size of 0.05°. Rietveld profile refinements were performed using the GSAS program, employing a pseudo-Voigt peak shape function. Cooling for low-temperature scans was performed using a closed cycle refrigerator. DC magnetization measurements were collected on a Quantum Design MPMS 7 SQUID magnetometer from 5 to 320 K on samples cooled and measured in an applied field of 1 T. Magnetotransport measurements were performed in an Oxford Instruments Maglab 2000 system with applied fields of up to 7 T and a temperature range of 2−320 K. Powdered samples were made into pellets, sintered, and measured using the standard four-probe technique with the connections made with gold wiring and platinum paint.

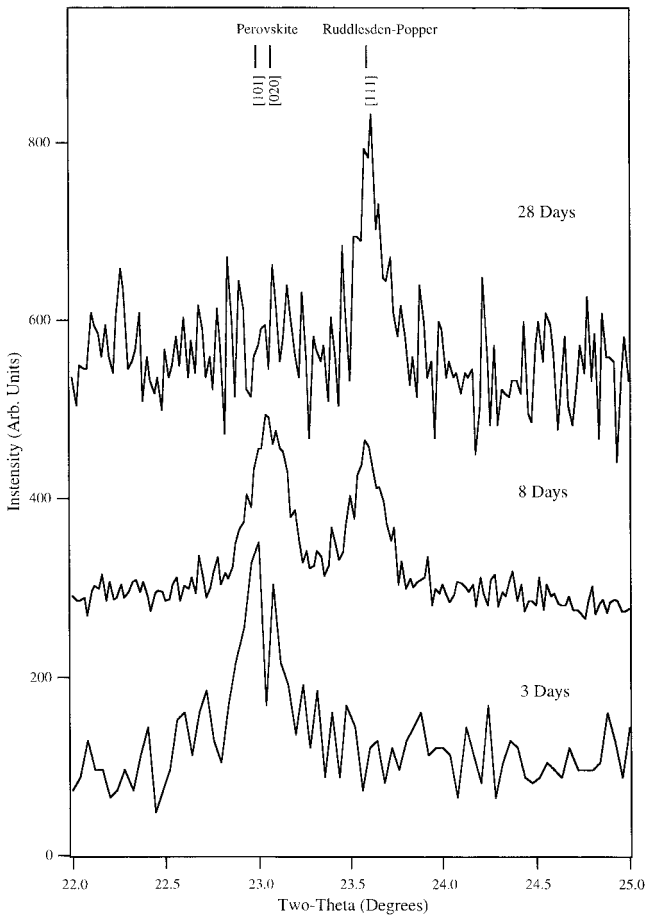

Figure 1. X-ray diffraction of $LaCa_2Mn_2O_7$ between 22° and 25° 2θ taken as a function of reaction time. The initial perovskite can be seen to transform to the Ruddlesden−Popper phase over a 28-day period.

Synthesis

Much care has to be taken with the synthesis of Ruddlesden−Popper phases as they are often close in energy to the other members of the series, as well as the perovskite phase. The progress of the reaction of starting materials to $LaCa_2Mn_2O_7$ was monitored by X-ray diffraction. The strongest X-ray scattering feature is comprised of the [020], [002], and [511] reflections. (The reflections are given with respect to the *Cmcm* unit cell described later, where *a* is the long axis.) They are at almost identical *d* spacing and can only be separated by high-resolution studies. They are also coincident with the main perovskite reflection and therefore were not useful in the initial characterization. The layered members of the Ruddlesden−Popper series are most conveniently distinguished by the presence of their [200] reflection. This reflection (at around 9° for the $n = 2$ member) is often relatively weak in the manganate systems, see for example the pattern for $Sr_2YMn_2O_7$.[12] However, for $LaCa_2Mn_2O_7$, the [200] reflection is one of the most intense reflections and can be used to monitor the growth of the Ruddlesden−Popper phase.

(10) Battle, P. D.; Blundell, S. J.; Green, M. A.; Hayes, W.; Honold, M.; Klehe, A. K.; Laskey, N. S.; Millburn, J. E.; Murphy, L.; Rosseinsky, M. J.; Samarin, N. A.; Singleton, J.; Sluchanko, N. E.; Sullivan, S. P.; Vente, J. F. *J. Phys.-Condens. Matter* **1996**, *8*, L.

(11) Battle, P. D.; Green, M. A.; Laskey, N. S.; Millburn, J. E.; Radaelli, P. G.; Rosseinsky, M. J.; Sullivan, S. P.; Vente, J. F. *Phys. Rev. B−Condens. Matter* **1996**, *54*, 15967.

(12) Battle, P. D.; Green, M. A.; Laskey, N. S.; Millburn, J. E.; Murphy, L.; Rosseinsky, M. J.; Sullivan, S. P.; Vente, J. F. *Chem. Mater.* **1997**, *9*, 552.

(13) Battle, P. D.; Green, M. A.; Laskey, N. S.; Kasmir, N.; Millburn, J. E.; Spring, L. E.; Sullivan, S. P.; Rosseinsky, M. J.; Vente, J. F. *J. Mater. Chem.* **1997**, *7*, 977.

(14) Battle, P. D.; Millburn, J. E.; Rosseinsky, M. J.; Spring, L. E.; Vente, J. F.; Radaelli, P. G. *Chem. Mater.* **1997**, *9*, 3136.

(15) Raychaudhuri, P.; Mitra, C.; Paramekanti, A.; Pinto, R.; Nigam, A. K.; Dhar, S. K. *J. Phys. Condens. Matter.* **1998**, *10*, L191.

(16) Asano, H.; Hayakawa, J.; Matsui, M. *Appl. Phys. Lett.* **1996**, *68*, 3638.

(17) Asano, H.; Hayakawa, J.; Matsui, M. *Phys. Rev. B−Condens. Matter* **1997**, *56*, 5395.

(18) Asano, H.; Hayakawa, J.; Matsui, M. *Appl. Phys. Lett.* **1997**, *70*, 2303.

(19) Asano, H.; Hayakawa, J.; Matsui, M. *Jpn. J. Appl. Phys. Part 2-Lett.* **1997**, *36*, L104.

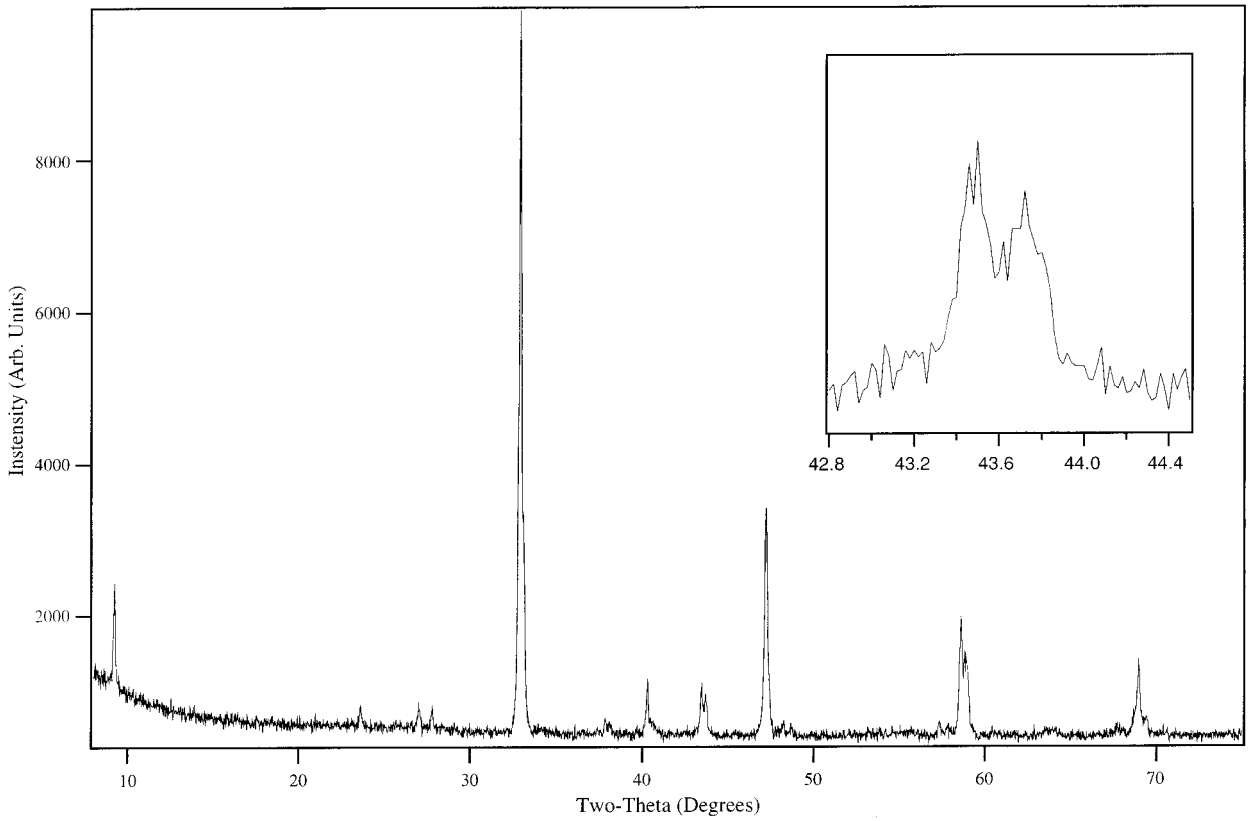

Figure 2. High-resolution X-ray diffraction pattern of $LaCa_2Mn_2O_7$ after 28 days synthesis period. Inset shows the splitting of the reflection at 43°.

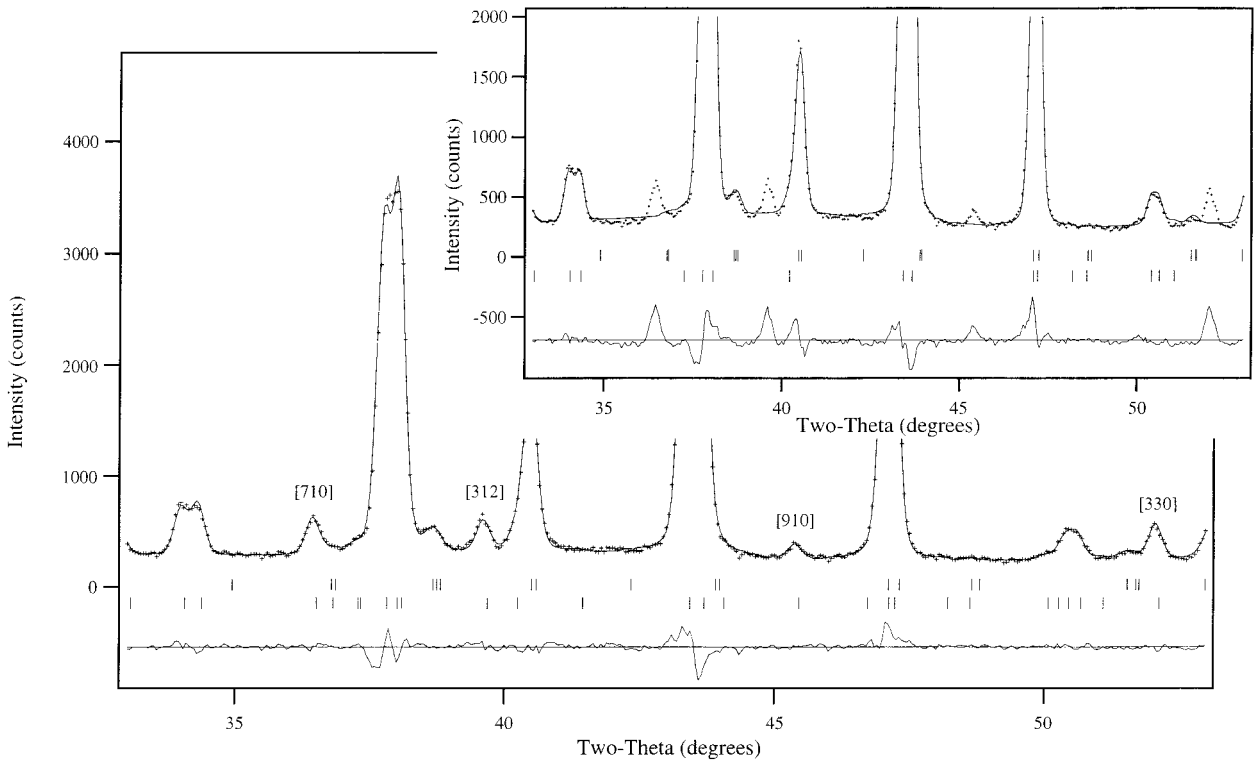

Figure 3. Observed, calculated, and difference plot of the powder neutron diffraction data at room-temperature fitted with a perovskite and a Ruddlesden−Popper phase. The Ruddlesden−Popper phase is described in a *Cmcm* space group with the [710], [312], [910], and [330] reflections appropriately fitted. The inset shows the same fit but with the Ruddlesden−Popper phase in a *Fmmm* space group indicating a number of missing reflections. The upper and lower tick marks refer to the perovskite and Ruddlesden−Popper phase, respectively.

The pairs of reflections around 27° (the [311] and [600]) and at 43° (the [620] and [602]), as well as the [400] at 18.3° and [111] at 23.6°, are also unique to the $n = 2$ phase.

The initial reaction product was indexed on a perovskite cell; no reflections associated with the Ruddlesden−Popper phase were observed. The reflections unique to the $n = 2$ phase, in particular the [200], took several days (>3 days) heating before being apparent in the X-ray diffraction pattern. To follow the perovskite to Ruddlesden−Popper reaction, extended X-ray diffraction scans from 22° to 25° were performed after each heating, which incorporates the [111] reflection of the Ruddlesden−Popper phase and a doublet ([101] and [020] reflections) from the perovskite. Although these reflections are extremely weak, there is no overlap between the perovskite and Ruddlesden−Popper peaks and they can be used to distinguish between them. Figure 1 shows the data after 3, 8, and 28 days. From around 5 days to 15 days, the ratio of these reflections rapidly changed, with them being equal at around 9 days. After 15 days, with most of the sample being the Ruddlesden−Popper phase, changes in the ratio were extremely slow. Only after 28 days was no perovskite phase detectable by X-ray diffraction. Synthesis was also attempted at different temperatures. Samples which were heated to higher temperatures (1400 °C or above) formed the perovskite structures and simple metal oxides alone. At lower temperatures (1300 °C or below) the perovskite structures formed initially but the transformation to the Ruddlesden−Popper phase was extremely slow and never went to completion.

Structure

The X-ray diffraction profile of $LaCa_2Mn_2O_7$ after 28 days of heating is shown in Figure 2. It is clear from the splitting of the reflections at around 32° and 43° (shown as an inset), that the symmetry is lower than the conventional $Sr_3Ti_2O_7$-type structure (space group $I4/mmm$). All reflections could be indexed on a doubled $\sqrt{2}a \times \sqrt{2}b \times c$ cell using an orthorhombic space group with lattice parameters $a = 5.41$ Å, $b = 5.46$ Å, and $c = 19.27$ Å. LeBail extraction within the GSAS program was used to test the goodness of fit of various space groups. All of the F-centered space groups containing a diamond glide plane, such as *Fddd*, failed to predict certain reflections. All reflections were predicted in the *Fmmm* space group and full Rietveld refinement gave a satisfactory agreement with the experimental data ($\chi^2 = 1.12$).

The *Fmmm* space group was used as the initial model for refinement of the room-temperature neutron diffraction data, which was performed on the same sample as was used for the X-ray studies. There were clear gross differences between the *Fmmm* model and the observed data, indicating a further reduction of symmetry and/or the presence of an impurity phase. Indexing of a subset of the extra reflections led to the identification of a second phase with the perovskite-type structure, which could not be seen in the X-ray data. This perovskite phase was included into the refinement using the *Pnma* space group and led to a significant drop in the goodness of fit factors. The lattice parameters of the perovskite impurity phase were refined to be $a = 5.4421$ Å, $b = 7.6839$ Å, and $c = 5.4585$ Å. Within this second phase the lattice parameters, atomic positions, ratios of lanthanum to calcium on the A site and the peak shape parameters were allowed to vary independently, as well as a phase fraction parameter. A section of the fit with a Ruddlesden−Popper phase refined in the *Fmmm* space group and a perovskite phase is shown as an inset in Figure 3. A number of reflections were still not yet accounted for by these two phases; however, all of these additional reflections could be indexed within the $\sqrt{2}a \times \sqrt{2}b \times c$ Ruddlesden−Popper cell, implying a reduction from the *Fmmm* space group. Analysis of the reflection conditions shows the *Fmmm* conditions; *hkl*: $h + k$, *hkl*, $k + l$ inappropriate for this material, but no exception to the condition *hkl*: $k + l$ was found. The presence of the [1 4 0] implied a reduction in the reflection condition *hk*0: $h + k$ to *hk*0: k. The 0*kl*: $k+l$ was maintained, with 0*kl*: k,l being ruled out due to the presence of the [0 3 13]. This implies the symmetry must be reduced to *Amam*. This was transformed to the more conventional setting of *Cmcm* with a lattice parameter of $a = 19.2720$ Å, $b = 5.4650$ Å, and $c = 5.4132$ Å.

The room-temperature powder neutron diffraction data were refined in the *Cmcm* space group with a perovskite impurity phase and gave an excellent fit to the remaining reflection. The peak shape was initially Gaussian with a Lorentzian component added in the final stages of the refinement. A section of the fit is shown in Figure 3. The refined atomic positions are given in Table 1. A mixture of isotropic (La, Ca, and Mn) and anisotropic (O) thermal parameters were used, which are given in Table 2, and some selected bond distances and angles are listed in Table 3. The A site composition of the perovskite phase refined to give the overall formula of $La_{0.65}Ca_{0.35}MnO_3$. Comparison with various members of the $La_{1-x}Ca_xMnO_3$ phase reported in the literature shows that the *b* parameter is sensitive

Table 1. Structural Parameters of $LaCa_2Mn_2O_7$ at 12 K and Room Temperature in the *Cmcm* Space Groups

	T (K)	
	12	300
a (Å)	19.2020(9)	19.2722(8)
b (Å)	5.4561(3)	5.4651(2)
c (Å)	5.4150(3)	5.4132(2)
V (Å^3)	567.32(5)	570.14(4)
La/Ca (0.5, *y*, 0.75)		
y	0.2497(12)	0.2478(10)
La occupancy	*a*	0.66(2)
Ca occupancy	*a*	0.34(2)
La/Ca (*x*, *y*, 0.75)		
x	0.6844(2)	0.6842(2)
y	0.2652(11)	0.2591(10)
La occupancy	*a*	0.17(1)
Ca occupancy	*a*	0.83(1)
Mn (*x*, *y*, 0.75)		
x	0.6003(3)	0.6000(3)
y	0.7500(20)	0.7498(17)
O(1) (0.5, *y*, 0.75)		
y	0.8014(12)	0.7991(10)
O(2) (*x*, *y*, 0.75)		
x	0.6987(2)	0.6987(1)
y	0.7094(11)	0.7082(9)
O(3) (*x*, 0.0, 0.0)		
x	0.3928(2)	0.3933(1)
O(4) (*x*, 0.5, 0.0)		
x	0.5883(2)	0.5883(2)
wR_p	5.80%	4.78%
R_p	4.50%	3.89%
R_F^2	3.94%	3.27%
χ^2	2.28	1.50

[a] Fixed at value determined at room temperature.

Table 2. Thermal Factors Parameters for $LaCa_2Mn_2O_7$ at (a) 12 K and (b) Room Temperature[a]

	U_{iso} (Å^2)	U_{11} (Å^2)	U_{22} (Å^2)	U_{33} (Å^2)	U_{13} (Å^2)	U_{23} (Å^2)
			a. 12 K			
La/Ca (0.5, *y*, 0.75)	0.55(10)					
La/Ca (*x*, *y*, 0.75)	1.27(12)					
Mn (*x*, *y*, 0.75)	1.20(11)					
O(1) (0.5, *y*, 0.75)		0.01(30)	0.23(41)	3.00(41)		
O(2) (*x*, *y*, 0.75)		0.36(23)	1.53(33)	3.47(34)	−0.19(16)	
O(3) (*x*, 0.0, 0.0)		1.03(24)	2.13(25)	1.74(32)		1.60(35)
O(4) (*x*, 0.5, 0.0)		1.10(19)	0.81(21)	1.84(29)		0.83(30)
			b. Room Temperature			
La/Ca (0.5, *y*, 0.75)	0.97(13)					
La/Ca (*x*, *y*, 0.75)	1.53(12)					
Mn (*x*, *y*, 0.75)	1.19(11)					
O(1) (0.5, *y*, 0.75)		0.47(25)	−0.16(33)	3.01(32)		
O(2) (*x*, *y*, 0.75)		0.06(17)	1.91(26)	2.00(22)	0.20(13)	
O(3) (*x*, 0.0, 0.0)		1.39(20)	2.41(22)	1.46(25)		−0.47(31)
O(4) (*x*, 0.5, 0.0)		2.11(18)	1.55(18)	1.09(22)		0.11(25)

[a] At both temperatures, anisotropic thermal parameters were used to describe oxygen atoms, and all other atoms described by isotopic thermal parameters.

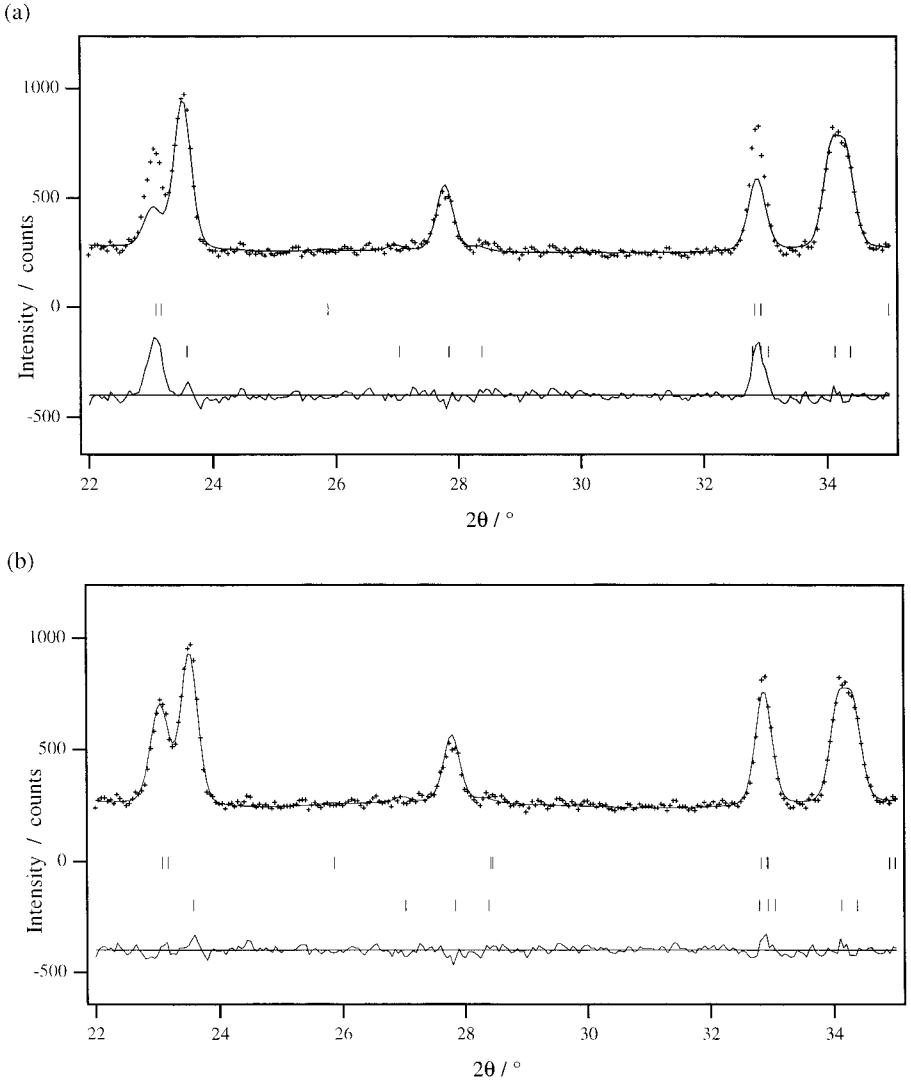

Figure 4. (a) Observed, calculated, and difference plot of the powder neutron diffraction data at 12 K fitted with a Ruddlesden−Popper phase and a perovskite phase without magnetic scattering and (b) the identical fit but with magnetic scattering included in the perovskite phase.

to composition. The value of $b = 7.6839$ Å estimates a composition for the refined perovskite phase to be $x \approx 0.4$. This is close to that obtained in the refinement itself, giving confidence in the accuracy of the composition. The weighted phase fraction was refined to be 88.6% Ruddlesden−Popper and 11.4% perovskite phase. Fractional occupancy of the two La and Ca sites in the Ruddlesden−Popper phase were refined with a constraint included to maintain a total site occupancy of 1 for both sites and well as an overall composition of

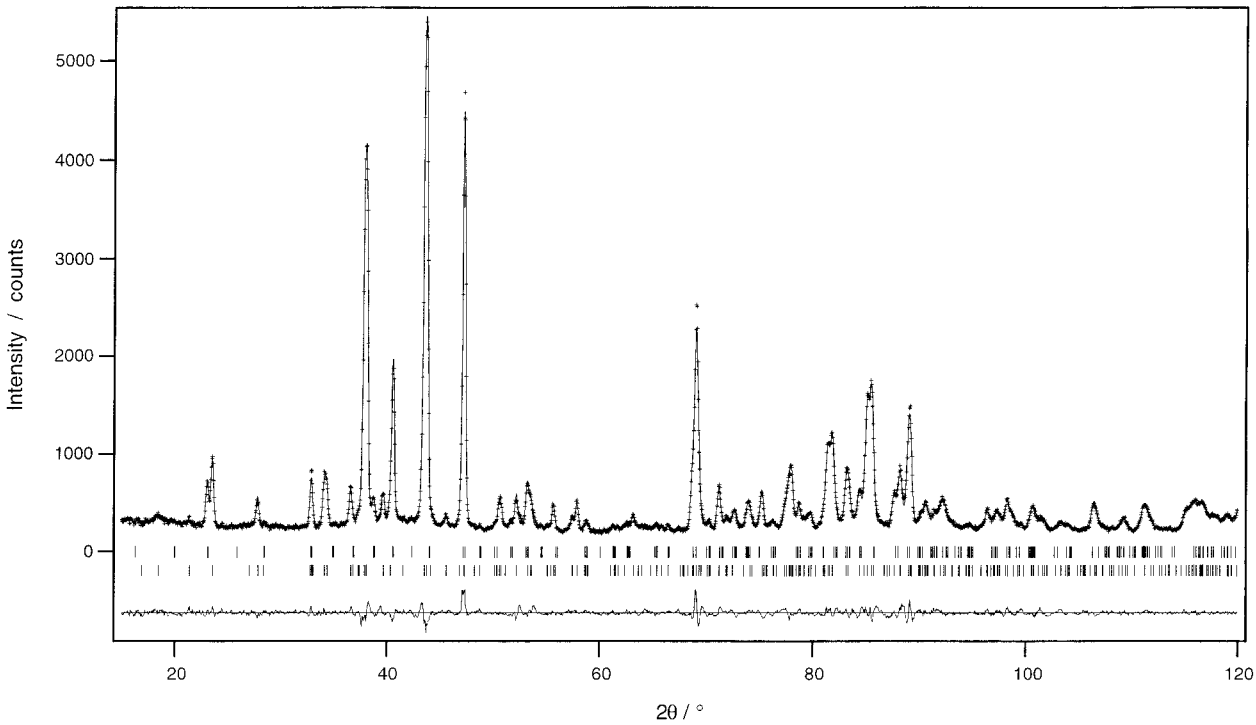

Figure 5. Observed, calculated, and difference plot of the powder neutron diffraction profiles at 12 K fitted with a perovskite and a Ruddlesden−Popper phase in the *Cmcm* space group. The upper and lower tick marks refer to the perovskite and Ruddlesden−Popper phase, respectively.

Table 3. Some Selected Bond Distances (Å) and Angles (deg) for $LaCa_2Mn_2O_7$ at 12 K and Room Temperature

	T (K)	
	12	300
Mn−O(1)	1.946(5)	1.945(6)
Mn−O(2)	1.915(6)	1.903(7)
Mn−O(3) × 2	1.928(7)	1.926(8)
Mn−O(4) × 2	1.935(7)	1.936(8)
La/Ca(1)[a]−O(1)	3.010(8)	3.013(7)
La/Ca(1)[a]−O(1)	2.446(8)	2.452(7)
La/Ca(1)[a]−O(1) × 2	2.722(1)	2.7187(8)
La/Ca(1)[a]−O(3) × 4	2.815(4)	2.810(4)
La/Ca(1)[a]−O(4) × 4	2.564(5)	2.575(4)
La/Ca(2)[a]−O(2)	3.045(6)	3.024(6)
La/Ca(2)[a]−O(2)	2.439(6)	2.470(6)
La/Ca(2)[a]−O(2)	2.266(5)	2.275(4)
La/Ca(2)[a]−O(2) × 2	2.7250(8)	2.7268(7)
La/Ca(2)[a]−O(3) × 2	2.474(5)	2.462(4)
La/Ca(2)[a]−O(4) × 2	2.622(5)	2.641(4)
O(1)−Mn−O(2)	178.9(6)	178.4(8)
O(1)−Mn−O(3)	88.20(28)	88.09(34)
O(1)−Mn−O(4)	89.01(34)	89.1(4)
O(2)−Mn−O(3)	90.98(31)	90.8(4)
O(2)−Mn−O(4)	91.80(29)	92.03(35)
O(3)−Mn−O(4)	177.2(4)	177.2(5)
O(3)−Mn−O(4)	89.01(34)	90.90(2)
O(3)−Mn−O(3)	89.1(4)	89.3(5)
Mn−O(3)−Mn	172.3(4)	172.1(5)
Mn−O(4)−Mn	166.7(4)	166.4(5)

[a] Site (1) at La/Ca (0.5, *y*, 0.75) and site (2) at La/Ca (*x*, *y*, 0.75).

$LaCa_2Mn_2O_7$. This resulted in cation occupancy refined to be 68% La and 32% Ca on the (0.5, *y*, 0.75) site and 16% La and 84% Ca on the (*x*, *y*, 0.75) site, implying a preference for the larger La ions to be situated in the 12-coordinated site between the Mn−O sheets and the Ca ions to lie in the 9-coordinated site in the rock salt layers. Occupancy of the oxygen sites was refined but no evidence for vacancies was found so these parameters were removed. Lower symmetry space groups with reduced reflection conditions such as $C222_1$ and *Cmmm* were attempted but the atom positions were always too unstable for the refinement to converge.

The room-temperature refined parameters were used as the starting model for the 12 K data with the fractional occupancy of the La and Ca sites constrained to those obtained at room temperature for both the Ruddlesden−Popper and perovskite phases. There were no additional reflections in either of the two phases, which would imply a further low temperature distortion. However, the fit to the perovskite phase was considerably worse than in the room temperature data. This was particularly evident in the group of peaks at 23.1° and 32.9°, shown in Figure 4a, which has substantially increased intensity over the pattern obtained at room temperature. Much improvement to the fit, particularly to these two reflections, was observed when a ferromagnetic component was included in the model for the perovskite phase, as previously reported for similar systems.[20] Figure 4b shows a section of the fit with the magnetic scattering included. The value of Mn moment was refined to be 4.9(2) μ_B. The spin-only contribution to the Mn moment in the perovskite phase, assuming a formula of $La_{0.65}Ca_{0.35}MnO_3$, is calculated to be 4.54 μ_B. The observed value refined in the neutron diffraction experiments is slightly higher than that expected. The reason for this discrepancy is probably due to large inaccuracies incurred because of the small phase fraction of the perovskite phase, the perovskite composition not being exactly known and the overlap of the perovs-

(20) Huang, Q.; Santoro, A.; Lynn, J. W.; Erwin, R. W.; Borchers, J. A.; Peng, J. L.; Ghosh, K.; Greene, R. L. *Phys. Rev. B.* **1998**, *58*, 2684.

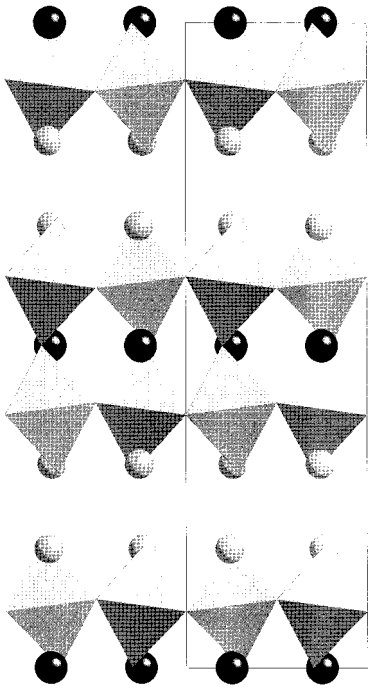

Figure 6. Room-temperature structure of $LaCa_2Mn_2O_7$ as determined from powder neutron diffraction. The smaller light circles represent the predominately Ca site and the darker larger circles represent the predominately La site.

kite reflections with those associated with the Ruddlesden−Popper phase. There were no significant changes in the intensity to any of the reflections, or the appearance of additional reflections, associated with the Ruddlesden−Popper phase between the ambient and low-temperature profiles, which rules out ferromagnetic or antiferromagnetic long-range magnetic ordering in this phase. Figure 5 shows the fit to the 12 K data over the complete angular range and includes the *Cmcm* Ruddlesden−Popper phase and a *Pnma* perovskite phase with magnetic scattering. The final refined structure of the Ruddlesden−Popper phase, $LaCa_2Mn_2O_7$, is shown in Figure 6 and shows significant rotation of the Mn−O octahedra with respect to the ideal *Fmmm* space group. In addition to the octahedral tilting, the *Cmcm* space group allows the Mn−O octahedra to have anisotropic Mn−O bond distances, such that those in the *ab* plane are split into a 2 × 2 arrangement with individual distances for the two bonds along the *c* direction (Figure 7). Interestingly, although this flexibility in bond distances is allowed by symmetry, in the case of both temperatures there is very little distortion of the Mn−O octahedra. For example, the values at 12 K are 1 × 1.946 Å, 1 × 1.915 Å, 2 × 1.928 Å, and 2 × 1.935 Å.

Magnetic and Magnetotransport Measurements

Magnetization measurements indicate a weak ferromagnetic component with a $T_c \approx 250$ K shown in Figure 8a. This is approximately the degree of magnetization expected from the ferromagnetic component refined in the perovskite impurity and gives further evidence that the origin of this transition is the perovskite impurity phase rather than the majority Ruddlesden−Popper phase. The transition temperature of 250 K is also indicative of the perovskite phase, see for example the review by Rao et al.[2] To examine the relationship

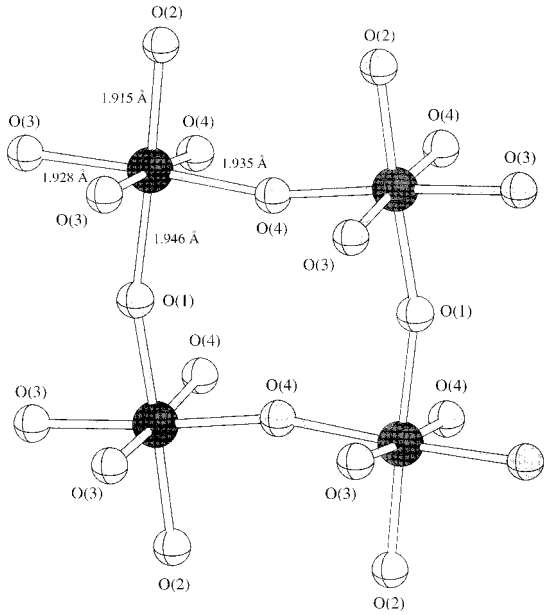

Figure 7. The Mn−O bond coordination at 12 K obtained from powder neutron diffraction showing significant rotation of the Mn−O octahedra, but relatively isotropic bond distances.

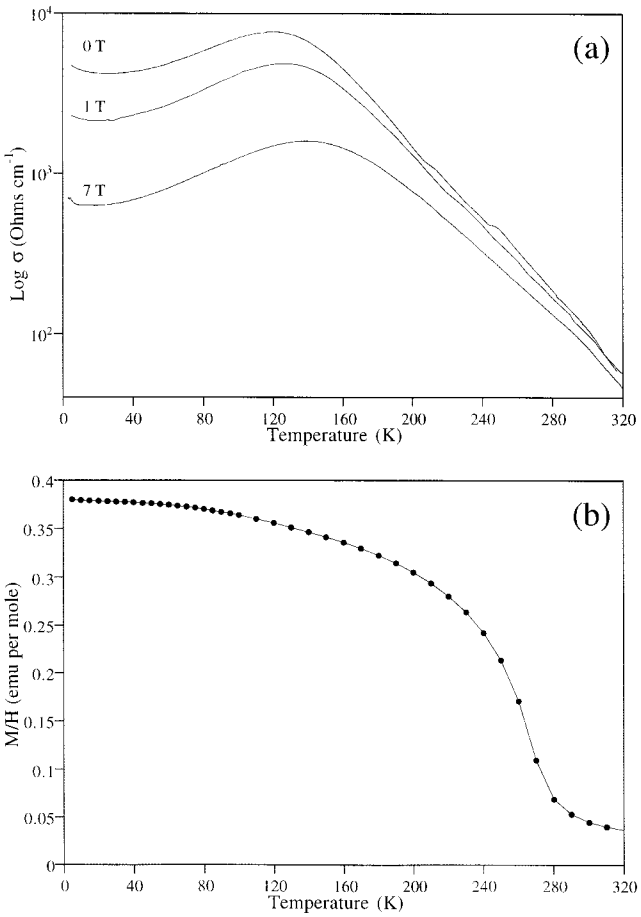

Figure 8. (a) The temperature dependence of M/H of the sample, calculated assuming a mixture of 88.6% of $LaCa_2Mn_2O_7$ and 11.4% $La_{0.65}Ca_{0.35}MnO_3$ phases, cooled, and measured in an applied field of 1T. (b) The log of the resistivity of $LaCa_2Mn_2O_7$ and perovskite phase under an applied field of 0, 1, and 7 T.

between the amount of perovskite phase and the magnetization, a number of magnetic measurements

were performed during the reaction time. It was found that the saturation moment reduced as the reaction proceeded, implying that the loss of magnetization was due to the decreasing amount of perovskite impurity. Magnetotransport measurements were performed on the $LaCa_2Mn_2O_7$ sample used in the neutron and X-ray experiments. The conductivity as a function of applied magnetic field is shown in Figure 8b. The measurements show metallic temperature dependence below 150 K and semiconducting properties above. It is important to note the high resistivity throughout the whole temperature regime and the relatively small reduction of resistance at 150 K; both of which are uncharacteristic of a transition associated with double exchange induced ferromagnetism alone. It may be possible that the conductivity data is a combination of semiconducting properties associated with the Ruddlesden−Popper phase and a small amount of perovskite impurity which is metallic below its ferromagnetic transition of around 250 K. Application of a magnetic field significantly reduces the resistivity, although it retains a similar temperature dependence in all fields. The magnetoresistance effect (MR) (calculated using the equation $MR = R(0) - R(H)/R(0)$) was found to be around 90% at 7 T within the temperature range of 5 to 150 K. Above 150 K, a gradual reduction of MR occurs to a value of around 12% at 320 K. However, the perovskite impurity makes confident interpretation of these data impossible.

In conclusion, many of the main reflections of the perovskite and Ruddlesden−Popper phases, which are strongly overlapping in the X-ray diffraction data, are distinct in the neutron profiles, allowing unique indexing to be performed. This has allowed the identification of two phases within the sample and consequently accurate characterization of each phase. It has revealed a complex orthorhombic structure and absence of long-range magnetic ordering in the Ruddlesden−Popper phase and allowed a ferromagnetic transition in the susceptibility data to be assigned to the perovskite impurity. The perovskite impurity may also have been present in previous studies and this mixture of phases could be the cause of the unusual magnetoresistance effects reported.

Acknowledgment. We thank EPSRC for an Advanced Fellowship (M.A.G.) and NIST for provision of neutron beam time. Drs. M. J. Rosseinsky, P. D. Battle, and J. Vente are thanked for many useful discussions.

CM991094I